

Folding Units Govern the Cytochrome *c* Alkaline Transition

Linh Hoang*, Haripada Maity, Mallela M. G. Krishna, Yan Lin and S. Walter Englander

The Johnson Research Foundation, Department of Biochemistry and Biophysics University of Pennsylvania School of Medicine Philadelphia, PA 19104-6059 USA

The alkaline transition of cytochrome *c* is a model for protein structural switching in which the normal heme ligand is replaced by another group. Stopped flow data following a jump to high pH detect two slow kinetic phases, suggesting two rate-limiting structure changes. Results described here indicate that these events are controlled by the same structural unfolding reactions that account for the first two steps in the reversible unfolding pathway of cytochrome *c*. These and other results show that the cooperative folding-unfolding behavior of protein foldons can account for a variety of functional activities in addition to determining folding pathways.

© 2003 Elsevier Ltd. All rights reserved

Keywords: protein folding; cytochrome *c*, alkaline transition; hydrogen exchange; protein function

*Corresponding author

Introduction

The present work applies a hydrogen exchange method to the study of a protein structural transition, the alkaline transition experienced by equine cytochrome *c* (Cyt *c*) at high pH. Although the alkaline transition of Cyt *c* was identified some 60 years ago,¹ the underlying mechanism is still unclear.² The high pH transition replaces the buried Met80-S to heme Fe ligand with an external lysine. A similarly reconfigured state may play a role in some physiologically important interactions of Cyt *c* at neutral pH (cytochrome oxidase,^{3,4} cardiolipin,^{5,6} lipid membranes;^{7,8} reviewed by Rosell *et al.*⁹).

Stopped-flow spectroscopic studies of Cyt *c* following a jump to high pH reveal two kinetic steps.¹⁰ An initial step involves the deprotonation of some unidentified buried group, controlled by a structural event that allows some solvent species to enter the protein. The second step physically removes the normal heme ligand and brings a protein surface residue in to replace it. The present

study identifies two structural reactions that appear to control these two steps.

Previous work using native state hydrogen exchange methods (NHX) has shown that the small Cyt *c* protein (104 residues) is composed of five structural units (foldons) that engage in reversible unfolding and refolding behavior,^{11–14} even under fully native conditions. NHX methods can identify each folding unit at amino acid resolution and can measure its equilibrium stability and reversible unfolding and refolding rate.^{11–22} These same unit foldons appear to determine a stepwise pathway that carries unfolded Cyt *c* to its native state.^{11,14–19} The present study correlates the first two reactions in the reversible unfolding pathway with the two structural steps that determine the alkaline transition.

Results

The equilibrium alkaline transition

Figure 1 depicts the equilibrium alkaline transition in several equine Cyt *c* variants, measured by the loss of the 695 nm charge transfer band which is specific for the native Met80-S to heme Fe ligation. The transition pK_a for a recombinant pWT Cyt *c* (His26Asn/His33Asn) is 9.1 (Figure 1(a)). The likely high pH replacement ligands are the proximal lysine residues at positions 72, 73, and 79.^{23,24} When these three lysine residues are

Abbreviations used: Cyt *c*, equine cytochrome *c*; WT, wild-type; pWT, recombinant pseudo wild-type cytochrome *c* (His26Asn, His33Asn); foldon, cooperative folding/unfolding unit; HX, hydrogen exchange; GdmCl, guanidinium chloride; HAR, homoarginine; N-yellow, nested yellow.

E-mail address of the corresponding author: lhoang@mail.med.upenn.edu

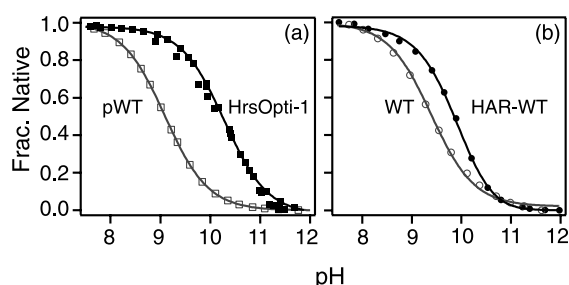


Figure 1. Equilibrium alkaline transition measured by CD or absorbance at 695 nm (20 °C). Data are fit by a one-proton titration curve. (a) Titration of pWT Cyt *c* compared to a variant (HrsOpti-1) with the normal replacement ligands removed by mutation (Lys72Gln/Lys73Ala/Lys79Arg). (b) Titration of WT equine Cyt *c* compared to a variant with all of the lysine residues blocked by guanidination to form homoarginine Cyt *c* (HAR-WT).

mutated to non-titratable residues the pK_a for the transition rises to 10.3. Similarly, Rosell *et al.*⁹ found a pK_a of 10.5 (up from 8.7) when the same lysine residues were chemically blocked in yeast iso-1-Cyt *c*. These results favor the vicinal lysine residues as the normal misligating groups.

Figure 1(b) shows another example. When all of the lysine residues in WT equine Cyt *c* are blocked by guanidination to form homoarginine (HAR), the pK_a for the alkaline transition rises from 9.35 to only 9.9. Similar results with all of the lysine residues blocked in various ways have been taken to suggest that non-lysine residues may be necessary to explain the alkaline transition (reviewed by Rosell *et al.*⁹). However, these multiple modifications are seriously perturbing. The misligating group is different (high spin *versus* low spin).²⁵ Also kinetic studies show that all of the 695 nm absorbance is lost in a very fast phase that does not limit at increasing pH, and then some absorbance slowly recovers (data not shown). Unmodified Cyt *c* behaves very differently (Figure 2).

The present work focuses on the structure changes that lead to the replacement of the Met80-

S ligand in unmodified WT Cyt *c*. Work in our laboratory and others show that various groups are able to misligate to the heme. The conclusions reached here are most consistent with but do not depend on the view that the normal replacement ligand is drawn from the vicinal lysine residues.

Kinetics of the alkaline transition

Figure 2 shows stopped-flow results for the alkaline transition when WT equine Cyt *c* is mixed into high pH. The kinetics are biphasic.

A small fast phase reduces the amplitude of 695 nm absorbance by 15% in the range above pH ~ 10 . It disappears at lower pH. The rate of the fast phase decreases as pH rises, limiting at $16(\pm 3) s^{-1}$ at high pH. This phase registers the exposure and deprotonation of some buried group near the heme. The apparent pK_a of this group is below pH 10, indicated by the fact that the full 15% change is realized by pH 10.

The remaining A_{695} is then lost in a slower phase indicating the replacement of the Met80-S by another ligand. Again the amplitude (85%) is insensitive to pH > 10 . The rate of this phase increases as pH rises. It limits at $7.5(\pm 0.4) s^{-1}$. The pH dependence reflects the pre-equilibrium titration of a surface group with $pK_a \sim 11.4$, probably the misligating lysine (see equation (3) below).

Similar results were found by Kihara *et al.*¹⁰ and Hasumi.²⁶ A small rate discrepancy is due to the different temperatures used (20 °C *versus* 25 °C) and a small pH shift may be due to salt concentration (0.5 M *versus* 0.2 M). The data of Kihara *et al.*¹⁰ suggest a subsequent increase in the fast phase rate beginning above pH 12. This is due to the onset of a disruptive protein denaturation reaction described before.¹⁹ A more interesting increase in the fast phase rate occurs in some Cyt *c* homologs that have a stabilizing tyrosine residue at position 46.²⁷ As discussed below, this observation helps to identify the initial structural unfolding reaction.

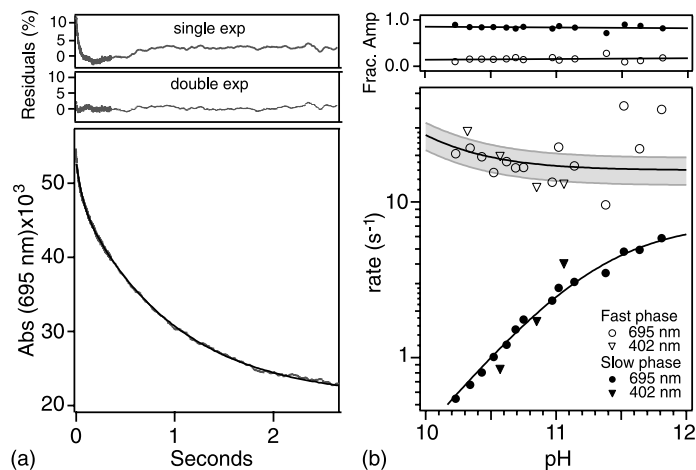
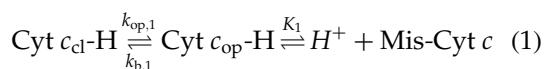


Figure 2. Kinetics of the alkaline transition of WT equine Cyt *c* followed by absorbance at 695 and 402 nm (20 °C). (a) A representative trace at pH 10.5 and the corresponding residuals for one and two exponential fits. (b) Amplitudes and rates of the fast and slow phases. Curves drawn for the faster phase show the range of uncertainty ($\pm 20\%$).

Alkaline transition models

Both of the observable kinetic steps in the alkaline transition involve a deprotonation and a rate-limiting structure change reaction. However, their dependence on pH is interestingly different. Figure 2(b) shows that the observed rate either falls or rises to reach the limiting rate. This is determined by whether the rate-limiting structure change occurs before or after the deprotonation step.

The limiting rate constant for the faster phase is 16 s^{-1} (Figure 2(b)), slower by far than one expects for deprotonation of a solvent-exposed group (over 10^6 s^{-1} in this pH range). Apparently the titrating group that generates the fast phase is protected by burial within the protein, and it is in the heme vicinity since its deprotonation perturbs the heme spectrum. Clearly, this group is not the surface lysine that acts as the eventual replacement ligand. In order to deprotonate an internal group, a structural gating reaction is required to allow some solvent base to enter the protein interior (OH^- or buffer base + solvating water molecules) and extract the proton. The opening of the structural gate must precede the deprotonation step, as in the reaction scheme in equation (1). In this case, the observed rate constant will decrease as pH rises, as is seen (Figure 2(b)), and it will limit at the effective structural opening rate, as in equation (2):

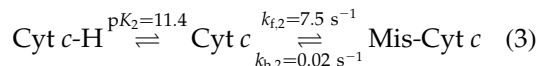


$$k_{\text{obs},1} = k_{\text{op},1} + k_{\text{b},1} \frac{[\text{H}^+]}{K_1 + [\text{H}^+]} \quad (2)$$

In equation (2), the observed rate is $k_{\text{obs},1}$, the structural opening rate that allows the deprotonation is $k_{\text{op},1}$, and the reverse reprotonation has a complex rate constant summarized here as $k_{\text{b},1}$. The observed rate decreases with pH because: (1) in a kinetic pH jump experiment, the rate measured represents a relaxation to the new equilibrium condition, given by the sum of the forward and backward rates; (2) in this case only the backward rate is pH-dependent and its contribution decreases as pH rises. (An interesting point is that, at low pH where the system equilibrates at less than full amplitude, the rate observed for approach to equilibrium is able to appear faster than the limiting opening rate.)

The much-studied slower phase of the alkaline transition, the misligation step itself, has generally been considered in terms of the reaction scheme in equation (3). Figure 2(b) shows that the misligation rate rises to a limiting value of 7.5 s^{-1} at high pH. This requires the prior (pre-equilibrium) deprotonation of the replacement ligand, presumably a surface lysine,^{2,28} with apparent $\text{p}K_{\text{a}}$ of 11.4. The parameters in equation (3) explain the apparent $\text{p}K_{\text{a}}$ of 9.35 for the equilibrium alkaline transition

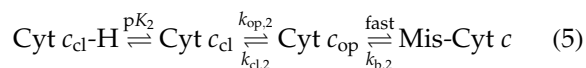
(Figure 1) as $\text{p}K_{\text{a}} = \text{p}K_2 - \log(k_{\text{f}}/k_{\text{b}})$:



In this case the observed rate constant, $k_{\text{obs},2}$, increases with pH and limits at the forward misligation rate. This is so because the forward rate is pH-dependent and increases with pH, as in equation (4). The backward deligation rate constant, $k_{\text{b},2}$, is much smaller:

$$k_{\text{obs},2} = k_{\text{f},2} \frac{K_2}{K_2 + [\text{H}^+]} + k_{\text{b},2} \quad (4)$$

In fact, the true reaction is slightly more complex. The misligation rate ($k_{\text{obs},2}$) is determined by a significant structure change necessary to physically remove the normal Met80-S ligand from the heme iron and bring the surface lysine into the buried heme site, as in equation (5). In this case, equation (4) still holds but the limiting forward rate constant is replaced by $k_{\text{op},2}$, the structural “opening” rate. The backward rate becomes more complex but it is slow and does not affect the measured $k_{\text{obs},2}$ except at very low pH:



In summary, each of the two steps observed in a kinetic alkaline transition experiment involves a deprotonation and a rate-limiting structure change reaction. The faster kinetic phase represents an internal deprotonation that is rate-limited by some prior structural gating reaction. The slower step represents the misligation reaction itself. It is rate-limited by some structure change that replaces the internal Met80-S ligand by a previously deprotonated surface lysine.

This work uses a kinetic version of the NHX method to characterize the two rate-limiting structural steps.

Reversible unfolding reactions by native state HX

Recent progress in hydrogen exchange has made it possible to detect and characterize transient unfolding reactions in protein molecules. The native state HX method is based on the thermodynamic principle that proteins must continually cycle through all of their higher energy partially unfolded forms, unfolding and refolding even under native conditions.

An equilibrium NHX method has identified five concerted unfolding units in Cyt *c* (foldons), and measured their equilibrium constants and sensitivity to denaturant.^{11,14} The unfolding/refolding units coincide with naturally cooperative elements of secondary structure, entire helices and entire Ω loops (see Figure 3(a)). A quantity of further work has shown that these units determine a stepwise

unfolding/refolding pathway,^{11,14,15,19} as diagrammed in Figure 3(b).

A kinetic version of the NHX experiment, done at relatively high pH (pH > 9) where HX is in the EX1 region, can measure the reversible unfolding rates of these units.^{19–22} Fortunately for the present investigation, the useful pH range of the kinetic NHX experiment is the same as the pH range in which the alkaline transition occurs. Figure 4 shows HX rate as a function of pH for a number of measurable Cyt *c* hydrogen atoms in the Nested-yellow (N-yellow) Ω loop and the Red Ω loop (see Figure 3(a)).

At lower pH (EX2 region), HX rates are governed by equilibrium structural unfolding reactions that intermittently expose the protected amide hydrogen atoms to transient contact with solvent. Here HX rate increases with pH because the chemical exchange reaction is catalyzed by OH⁻ ion (equation (6)). The pH offset of HX rates for the different amide protons in the EX2 region (see Figure 4) is due to differences in their intrinsic chemical HX rates, determined by neighboring side-chain inductive and blocking effects.^{29,30} At high pH, HX rates are ultimately limited by the rate of the unfolding reaction (EX1 condition) that exposes the hydrogen atoms to exchange (equation (7)). The limiting rates at high pH exhibit a small but negligible spread.

Unfolding reactions and the alkaline transition

Figure 4 compares the unfolding rates for two Ω loops with the two rate processes measured for the alkaline transition. The averaged unfolding rate for the N-yellow Ω loop protons at high pH is $17(\pm 2) \text{ s}^{-1}$ ($15\text{--}20 \text{ s}^{-1}$ total range). This compares with the rate measured for the fast phase of the alkaline transition in the same high pH region, $16(\pm 3) \text{ s}^{-1}$.

The averaged Red loop unfolding rate, $9(\pm 2) \text{ s}^{-1}$ ($7.5\text{--}10.8 \text{ s}^{-1}$ total range) matches the limiting rate of the misligation phase, $7.5(\pm 0.4) \text{ s}^{-1}$. The best agreement is found with residues Tyr74 ($7.5(\pm 0.7) \text{ s}^{-1}$) and Ile75 ($7.4(\pm 0.5) \text{ s}^{-1}$). These

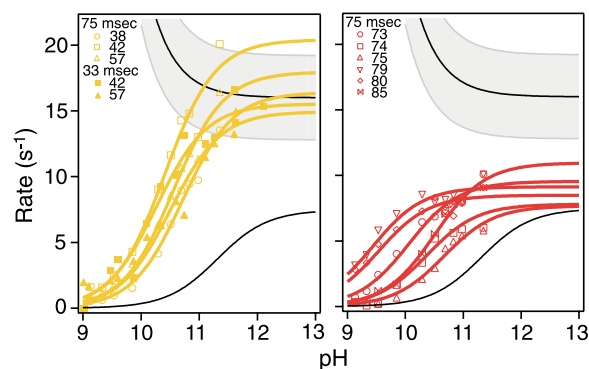


Figure 4. Structural unfolding rates (color) compared with the two phases in the alkaline transition (black; 20 °C in 0.5 M KCl). The limiting HX rates at high pH are the structural unfolding rates measured for protons in the N-yellow and Red Ω loops. Within each unit different protons initially reach the EX1 limit at somewhat different pH due to their different intrinsic rate constants.³⁰ HX pulse labeling times and protons measured are indicated.

so-called marker protons exchange only when the Red loop unfolds.^{11,19} In the EX2 region the non-marker amides exchange more rapidly, by way of local fluctuations. Their extrapolation into the EX1 region may receive a contribution from the local fluctuational pathways in addition to the dominant Red loop unfolding pathway. In any case, these differences are small and do not mask the final result.

These results suggest that the two alkaline transition reactions measured by stopped-flow are rate-limited by the transient unfolding of two unit loop structures (arrows in Figure 3(b)).

Discussion

Structure change in the alkaline transition and Red loop unfolding

The Red Ω loop (residues 71–85) protects the face of the heme that is misligated in the alkaline

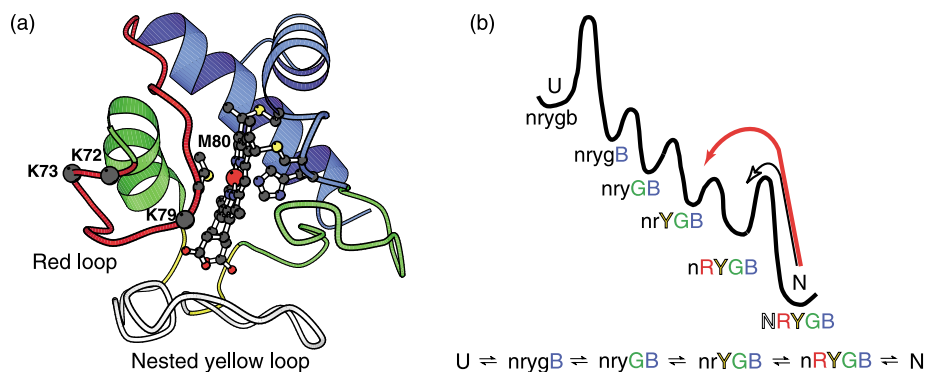


Figure 3. Cyt *c* and its folding free energy profile. (a) Equilibrium native state HX results have identified five concerted folding units, shown color-coded.^{11,14} (b) The Cyt *c* folding/unfolding pathway. Arrows show the unfolding reactions that appear to rate-limit the two kinetic steps seen at high pH in alkaline transition studies.

transition (Figure 3(a)). It contains the native heme ligand (Met80-S) and also the lysine residues (72, 73, 79) that appear to account for the high pH misligation in unmodified Cyt *c*. In order to physically remove Met80 from the heme and replace it with one of the surface lysine residues, a significant distortion of this segment seems necessary. In fact a solution NMR study of alkaline Cyt *c* misligated by Lys79 shows that the Red unit deviates strongly from the native structure whereas the N-yellow unit remains unchanged.³¹

Nelson & Bowler³² have previously suggested that the Red loop unfolding might mediate the alkaline transition. They found that these two equilibrium reactions have similar sensitivity to denaturant, expressed in terms of an *m* value ($m = \Delta(RT \ln K_u) / \Delta[\text{GdmCl}]$), which depends on the surface newly exposed to solvent in the unfolding. The *m* value for the equilibrium alkaline transition, 1.1–1.7 kcal/mol per M³² is close to the *m* value of 1.6 kcal/mol per M previously measured for Red unfolding by equilibrium native state HX.¹¹ In agreement, the present results show that the limiting rate for the misligation step matches the rate measured for the concerted unfolding of the Red loop at the same high pH condition.

The agreement of the kinetic rates, the agreement of the equilibrium *m* values, and the structural relationships required by the transition and seen by an NMR study consistently indicate that the naturally occurring Red loop unfolding represents the conformational rearrangement that limits the slower step in the alkaline transition.

Structure change in the alkaline transition and N-yellow loop unfolding

The faster phase of the alkaline transition produces a transient intermediate form that has an altered heme spectral absorbance, apparently caused by the titration of some nearby internal group. The deprotonation of an internal group requires the prior opening of some gating structure that would allow entry into the protein core of some solvent species able to act as a proton acceptor (OH⁻, buffer base). That this occurs is supported by the initial decrease in rate with pH (Figure 2(b); equation (2); see also Kihara *et al.*¹⁰).

The limiting rate for the fast phase of the alkaline transition matches the rate for unfolding of the N-yellow loop at the same high pH condition (Figure 4(a)). The unfolding of the N-yellow loop would allow solvent access to the heme crevice (see Figure 3(a)).

Saigo²⁷ found an additional sensitivity to pH for the fast phase rate in species that contain a tyrosine residue at position 46 (tuna, bonito, rhesus) but not in other species with Phe46 (horse, sheep, dog, pigeon). Tyr46 is in the N-yellow loop. It forms a stabilizing pH-sensitive H-bond. Its titration ($pK_a > 11$) increases the fast phase rate,²⁷ apparently because the disruption of this bond poten-

tiates the determining structure change, consistent with N-yellow unfolding.

In summary, the limiting gating rate for the internal deprotonation reaction is equal to the N-yellow unfolding rate. Destabilization of the N-yellow loop accelerates the deprotonation reaction.²⁷ N-yellow unfolding would open the heme crevice to invasion by solvent species. These observations support the conclusion that the naturally occurring N-yellow loop unfolding represents the conformational gating reaction that allows the deprotonation of some buried heme-related group, seen as an initial heme spectral change in kinetic alkaline transition experiments.

A general implication

It seems most noteworthy that the same two reversible unfolding reactions that determine the Cyt *c* alkaline transition represent the first two steps in the Cyt *c* unfolding pathway (Figure 3(b)). The same steps may also limit the binding of exogenous ligands to the heme group.³³ The accompanying work¹⁴ notes the involvement of the N-yellow loop in other structural and evolutionary actions. These results indicate that the foldon substructure of proteins, and particularly their naturally occurring reversible unfolding behavior, can act to determine not only folding/unfolding pathways but also a number of other important behaviors.

Materials and Methods

Materials

Equine Cyt *c* was from Sigma Chemical Co. (WT Cyt *c*). All experiments were done at 20 °C with 0.5 M KCl to minimize charge effects.

Homoarginine modified WT Cyt *c* was prepared as described by Hettinger *et al.*³⁴ Complete modification of all 19 lysine residues was confirmed by mass spectrometry and purity was verified by SDS/polyacrylamide gel electrophoresis.

The recombinant pWT Cyt *c* used has the potentially misligating histidine residues removed (His26Asn/His33Asn).³⁵ In a selectively modified pWT protein (HrsOpti-1) the three lysine residues thought to account for the normal alkaline transition are replaced by mutation (Lys72Gln/Lys73Ala/Lys79Arg), a Gln residue blocks the N terminus by spontaneous cyclization, and a near terminal proline contributes to stability (Val3Pro).

Equilibrium titration

Equilibrium pH titrations measured by CD and absorbance at 695 nm (5 nm bandwidth) used an automated Microlab 500 series titrator and continuous pH measurement in an AVIV CD Spectrometer model 202, regulated at 20 °C. The titrator added incremental volumes of NaOH, 0.5 M KCl (total added volume < 50 μl) to 2 ml of 0.4 mM protein in 0.5 M KCl, 10 mM KPO₄, 10 mM Bicine, 10 mM Caps. For each data point, equilibration

time was three minutes and the signal was averaged for 30 seconds.

Stopped-flow kinetics

Stopped-flow kinetics used a Biologic SFM-4 instrument (20 °C). Syringes 1 and 2 contained buffers at pH 9 and 12, with 50 mM Caps, 0.5 M KCl. Syringe 3 contained 0.7 mM protein (0.5 M KCl, 10 mM KPO₄, pH 6). The protein was diluted tenfold with incremental mixes of syringes 1 and 2 to set pH, measured after collection. Data analysis used Igor Pro 4.0.

Kinetic native state hydrogen exchange

Hydrogen-bonded amides experience dynamic opening and closing reactions that separate the protecting hydrogen bond and allow hydrogen exchange with the bulk solvent. In steady state, the overall exchange rate (k_{ex}) is given by equation (6),^{36,37} where k_{op} and k_{cl} are opening and reclosing rates of the protecting H-bond and $k_{\text{ch}} = k_{\text{int}}[\text{OH}^-]$. k_{int} is an intrinsic second-order rate constant which depends on temperature, nearest neighbor inductive and blocking effects, and isotope effects:^{29,30,38}

$$k_{\text{ex}} = \frac{k_{\text{op}}k_{\text{ch}}}{k_{\text{cl}} + k_{\text{ch}}} \quad (6)$$

When $k_{\text{cl}} \ll k_{\text{ch}}$ (the EX1 monomolecular exchange limit), exchange rate is given by equation (7), allowing the measurement of structural opening rates:³⁷

$$k_{\text{ex}} = k_{\text{op}} \quad (7)$$

A native state strategy employs mild destabilants to promote larger structural unfoldings over local fluctuations^{11,19} so that they come to dominate the exchange measured. The high pH used in the present work to promote the alkaline transition and to make $k_{\text{ch}} \gg k_{\text{cl}}$ (EX1 condition) was adequate to serve this function for the Red loop unfolding.

The very fast HX rate obtained at high pH was measured by exposing the protein to the high pH condition for only a short time.^{20,21} A labeling pulse of either 33 or 75 ms was used for the data set described here.¹⁹ The H to ²H exchange that occurs during the labeling pulse was measured by 2D NMR using the cross-peak assignments of Feng *et al.*³⁹ for oxidized Cyt *c*.

Acknowledgements

This work was supported by research grants from the NIH and the Mathers Foundation.

References

- Theorell, H. & Akesson, A. (1941). Studies on cytochrome *c*. *J. Am. Chem. Soc.* **63**, 1812–1818.
- Wilson, M. T. & Greenwood, C. (1996). The alkaline transition in ferricytochrome *c*. In *Cytochrome c: A Multidisciplinary Approach* (Scott, R. A. & Mauk, A. G., eds), pp. 611–634, University Science Books, Sausalito.
- Dopner, S., Hudecek, J., Ludwig, B., Witt, H. & Hildebrandt, P. (2000). Structural changes in cytochrome *c* oxidase induced by cytochrome *c* binding. A resonance Raman study. *Biochim. Biophys. Acta*, **1480**, 57–64.
- Falk, K. E. & Angstrom, J. (1983). A 1H NMR longitudinal relaxation study of the interaction between cytochrome *c* and cytochrome *c* oxidase. *Biochim. Biophys. Acta*, **722**, 291–296.
- Soussi, B., Bylund-Fellenius, A. C., Schersten, T. & Angstrom, J. (1990). 1H NMR evaluation of the ferricytochrome *c*-cardiolipin interaction. Effect of superoxide radicals. *Biochem. J.* **265**, 227–232.
- Hildebrandt, P., Vanhecke, F., Buse, G., Soulimane, T. & Mauk, A. G. (1993). Resonance Raman study of the interactions between cytochrome *c* variants and cytochrome *c* oxidase. *Biochemistry*, **32**, 10912–10922.
- Hildebrandt, P. & Stockburger, M. (1989). Cytochrome *c* at charged interfaces. 2. Complexes with negatively charged macromolecular systems studied by resonance Raman spectroscopy. *Biochemistry*, **28**, 6722–6728.
- Hildebrandt, P., Heimburg, T. & Marsh, D. (1990). Quantitative conformational analysis of cytochrome *c* bound to phospholipid vesicles studied by resonance Raman spectroscopy. *Eur. J. Biophys.* **18**, 193–201.
- Rosell, F. I., Ferrer, J. C. & Mauk, A. G. (1998). Proton-linked protein conformational switching: definition of the alkaline conformational transition of yeast iso-1-ferricytochrome *c*. *J. Am. Chem. Soc.* **120**, 11234–11245.
- Kihara, H., Saigo, S., Nakatani, H., Hiromi, K., Ikeda-Saito, M. & Iizuka, T. (1976). Kinetic study of isomerization of ferricytochrome *c* at alkaline pH. *Biochim. Biophys. Acta*, **430**, 225–243.
- Bai, Y., Sosnick, T. R., Mayne, L. & Englander, S. W. (1995). Protein folding intermediates: native-state hydrogen exchange. *Science*, **269**, 192–197.
- Chamberlain, A. K. & Marqusee, S. (2000). Comparison of equilibrium and kinetic approaches for determining protein folding mechanisms. *Advan. Protein Chem.* **53**, 283–328.
- Bai, Y. & Englander, S. W. (1996). Future directions in folding: the multi-state nature of protein structure. *Proteins: Struct. Funct. Genet.* **24**, 145–151.
- Krishna, M. M. G., Lin, Y., Rumbley, J. N. & Englander, S. W. (2003). Cooperative omega loops in cytochrome *c*: role in folding and function. *J. Mol. Biol.* **331**, 29–36.
- Xu, Y., Mayne, L. & Englander, S. W. (1998). Evidence for an unfolding and refolding pathway in cytochrome *c*. *Nature Struct. Biol.* **5**, 774–778.
- Milne, J. S., Mayne, L., Roder, H., Wand, A. J. & Englander, S. W. (1998). Determinants of protein hydrogen exchange studied in equine cytochrome *c*. *Protein Sci.* **7**, 739–745.
- Bai, Y. (1999). Kinetic evidence for an on-pathway intermediate in the folding of cytochrome *c*. *Proc. Natl Acad. Sci. USA*, **96**, 477–480.
- Rumbley, J., Hoang, L., Mayne, L. & Englander, S. W. (2001). An amino acid code for protein folding. *Proc. Natl Acad. Sci. USA*, **98**, 105–112.
- Hoang, L., Bédard, S., Krishna, M. M. G., Lin, Y. & Englander, S. W. (2002). Cytochrome *c* folding pathway: kinetic native-state hydrogen exchange. *Proc. Natl Acad. Sci. USA*, **99**, 12173–12178.
- Arrington, C. B. & Robertson, A. D. (2000). Microsecond to minute dynamics revealed by EX1-type hydrogen exchange at nearly every backbone

- hydrogen bond in a native protein. *J. Mol. Biol.* **296**, 1307–1317.
21. Canet, D., Last, A. M., Tito, P., Sunde, M., Spencer, A., Archer, D. B. *et al.* (2002). Local cooperativity in the unfolding of an amyloidogenic variant of human lysozyme. *Nature Struct. Biol.* **9**, 308–315.
 22. Yan, S., Kennedy, S. & Koide, S. (2002). Thermodynamic and kinetic exploration of the energy landscape of *Borrelia burgdorferi* OspA by native-state hydrogen exchange. *J. Mol. Biol.* **323**, 363.
 23. Smith, H. T. & Millett, F. (1980). Involvement of lysines-72 and -79 in the alkaline isomerization of horse heart ferricytochrome *c*. *Biochemistry*, **19**, 1117–1120.
 24. Pollock, W. B., Rosell, F. I., Twitchett, M. B., Dumont, M. E. & Mauk, A. G. (1998). Bacterial expression of a mitochondrial cytochrome *c*. Trimethylation of lys72 in yeast *iso-1*-cytochrome *c* and the alkaline conformational transition. *Biochemistry*, **37**, 6124–6131.
 25. Stellwagen, E., Babul, J. & Wilgus, H. (1975). The alkaline isomerization of lysine-modified ferricytochrome *c*. *Biochim. Biophys. Acta*, **405**, 115–121.
 26. Hasumi, H. (1980). Kinetic studies on isomerization of ferricytochrome *c* in alkaline and acid pH ranges by the circular dichroism stopped-flow method. *Biochim. Biophys. Acta*, **626**, 265–276.
 27. Saigo, S. (1981). Kinetic and equilibrium studies of alkaline isomerization of vertebrate cytochromes *c*. *Biochim. Biophys. Acta*, **669**, 13–20.
 28. Davis, L. A., Schejter, A. & Hess, G. P. (1974). Alkaline isomerization of oxidized cytochrome *c*. Equilibrium and kinetic measurements. *J. Biol. Chem.* **249**, 2624–2632.
 29. Molday, R. S., Englander, S. W. & Kallen, R. G. (1972). Primary structure effects on peptide group hydrogen exchange. *Biochemistry*, **11**, 150–158.
 30. Bai, Y., Milne, J. S., Mayne, L. & Englander, S. W. (1993). Primary structure effects on peptide group hydrogen exchange. *Proteins: Struct. Funct. Genet.* **17**, 75–86.
 31. Assfalg, M., Bertini, I., Dolfi, A., Turano, P., Mauk, A. G., Rosell, F. I. & Gray, H. B. (2003). Structural model for an alkaline form of ferricytochrome *c*. *J. Am. Chem. Soc.* **125**, 2913–2922.
 32. Nelson, C. J. & Bowler, B. E. (2000). pH dependence of formation of a partially unfolded state of a Lys 73 → His variant of *iso-1*-cytochrome *c*: implications for the alkaline conformational transition of cytochrome *c*. *Biochemistry*, **39**, 13584–13594.
 33. Sutin, N. & Yandell, J. K. (1972). Mechanisms of the reactions of cytochrome *c*. Rate and equilibrium constants for ligand binding to horse heart ferricytochrome *c*. *J. Biol. Chem.* **247**, 6932–6936.
 34. Hettinger, T. P. & Harbury, H. A. (1964). Guanidated cytochrome *c*. *Proc. Natl Acad. Sci. USA*, **52**, 1469–1476.
 35. Rumbley, J. N., Hoang, L. & Englander, S. W. (2002). Recombinant equine cytochrome *c* in *Escherichia coli*: high-level expression characterization, and folding and assembly mutants. *Biochemistry*, **41**, 13894–13901.
 36. Linderström-Lang, K. U. (1955). Deuterium exchange between peptides and water. *Chem. Soc. Spec. Publ.* **2**, 1–20.
 37. Hvidt, A. & Nielsen, S. O. (1966). Hydrogen exchange in proteins. *Advan. Protein Chem.* **21**, 287–386.
 38. Connelly, G. P., Bai, Y., Jeng, M. F. & Englander, S. W. (1993). Isotope effects in peptide group hydrogen exchange. *Proteins: Struct. Funct. Genet.* **17**, 87–92.
 39. Feng, Y., Roder, H., Englander, S. W., Wand, A. J. & Di Stefano, D. L. (1989). Proton resonance assignments of horse ferricytochrome *c*. *Biochemistry*, **28**, 195–203.

Edited by C. R. Matthews

(Received 6 February 2003; received in revised form 15 May 2003; accepted 27 May 2003)